

# 500-Element Ultrasound Phased Array System for Noninvasive Focal Surgery of the Brain: A Preliminary Rabbit Study With Ex Vivo Human Skulls

Kullervo Hynynen,<sup>1\*</sup> Gregory T. Clement,<sup>1</sup> Nathan McDannold,<sup>1</sup> Natalia Vykhodtseva,<sup>1</sup> Randy King,<sup>1</sup> P. Jason White,<sup>1</sup> Shuki Vitek,<sup>2</sup> and Ferenc A. Jolesz<sup>1</sup>

**The aim of this study was to test a prototype MRI-compatible focused ultrasound phased array system for trans-skull brain tissue ablation. Rabbit thigh muscle and brain were sonicated with a prototype, hemispherical 500-element ultrasound phased array operating at frequencies of 700–800 kHz. An ex vivo human skull sample was placed between the array and the animal tissue. The temperature elevation during 20–30-sec sonications was monitored using MRI thermometry. The induced focal lesions were observed in  $T_2$  and contrast-enhanced  $T_1$ -weighted fast spin echo images. Whole brain histology evaluation was performed after the sonications. The results showed that sharp temperature elevations can be produced both in the thigh muscle and in the brain. High-power sonications (600–1080 W) produced peak temperatures up to 55°C and focal lesions that were consistent with thermal tissue damage. The lesion size was found to increase with increasing peak temperature. The device was then modified to operate in the orientation that will be used in the clinic and successfully tested in phantom experiments. As a conclusion, this study demonstrates that it is possible to create ultrasound-induced lesions in vivo through a human skull under MRI guidance with this large-scale phased array. Magn Reson Med 52: 100–107, 2004. © 2004 Wiley-Liss, Inc.**

**Key words:** MRI; minimally invasive surgery; brain; focused ultrasound; tissue ablation

Noninvasive tissue ablation using focused ultrasound has significant potential for the treatment of tumors, as demonstrated by recent clinical trials (1–3). In focused ultrasound surgery, acoustic energy is concentrated in a tumor or other target, sparing the surrounding tissue. The precisely focused mechanical energy can be utilized for thermal or mechanical tissue destruction. This procedure would be particularly beneficial for treating brain disorders, as it is noninvasive, does not cause bleeding, and does not damage surrounding tissue.

The promise of focused ultrasound brain surgery has attracted interest for many years, starting with animal experiments by Lynn and Putnam six decades ago (4). These initial tests revealed that the skull is a major barrier for ultrasound due to its high attenuation and reflection coef-

ficient. In addition, the heterogeneity and variable thickness of the bone structure were found to severely distort the propagating wave and thus prevent sharp focusing through the skull. Since that time it has been commonly accepted that focused ultrasound brain surgery requires an open craniotomy to allow the ultrasound beam to pass. Focused ultrasound brain surgery was studied in depth by the Fry brothers and their colleagues (5) and later by Lele (6). While the extensive studies performed by these groups demonstrated the potential of focused ultrasound brain surgery, the requirement of a skull window has prevented all but occasional, small clinical trials (7).

Recent advances in transducer, amplifier, and medical imaging technology as well as progress in ultrasound modeling have increased the feasibility of using focused ultrasound for noninvasive brain surgery. First, the development of large-scale, high-power phased arrays and the amplifiers to drive them (8,9) has made it possible to correct the beam distortions induced by the skull. By using such arrays with a large geometric gain, the energy loss in the highly attenuating skull can be overcome, and a sharp focus in the brain can be produced (10,11). Second, using the density and geometric information of the skull bone that can now be obtained with high-resolution CT scans, the phase corrections needed to produce this sharp focus can be calculated using ultrasound propagation models (12). Third, the development of MRI for temperature imaging (13) and its utilization in guiding, monitoring, and controlling of focused ultrasound beams (3,14) have greatly increased the accuracy of focused ultrasound surgery. Recent animal studies have shown that MRI can detect ultrasound-induced lesions in brain tissue (15,16). In addition, MRI can detect the location of the focal temperature elevation below the threshold for thermal damage (15), so the beam can be precisely aimed and functionally critical structures can be spared.

The ability of delivering highly focused ultrasound beams through the intact skull will also make ultrasound interventions beyond tissue coagulation possible. Focused ultrasound has been shown to be able to open the blood-brain barrier for targeted delivery of macromolecules into the brain (17). Such targeted drug delivery would allow for new neurologically potent agents to enter into the brain only at preselected locations. This would have many potential applications, including gene therapy, chemotherapy, and perhaps even in the implantation of cells into the brain via a vascular route. Similarly, this trans-skull sonication method may allow one to take advantage of the acceleration of thrombolysis (18). Ultrasound can also be

<sup>1</sup>Department of Radiology, Brigham and Women's Hospital, and Harvard Medical School, Boston, Massachusetts.

<sup>2</sup>InSightec Ltd., Tirat Carmel, Israel.

Grant sponsor: NCI; Grant number: CA76550; Grant sponsor: InSightec Ltd., Haifa, Israel; Grant sponsor NIH; Grant number: CA089017.

\*Correspondence to: Kullervo Hynynen, Ph.D., Department of Radiology, Brigham and Women's Hospital and Harvard Medical School, 75 Francis Street, Boston, MA 02115. E-mail: kullervo@bwh.harvard.edu

Received 1 August 2003; revised 9 February 2004; accepted 9 February 2004.

DOI 10.1002/mrm.20118

Published online in Wiley InterScience (www.interscience.wiley.com).

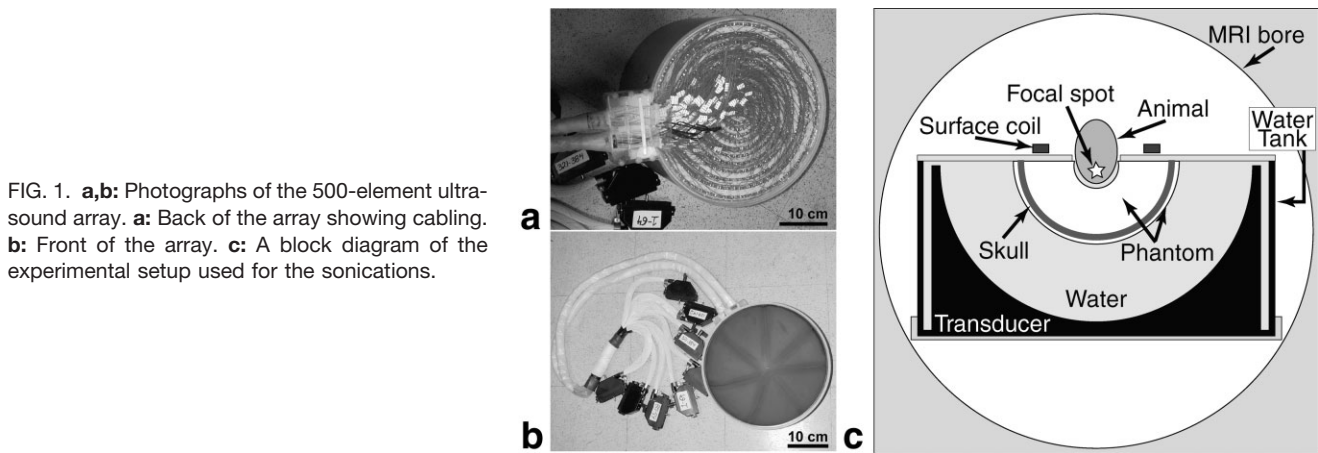


FIG. 1. **a,b**: Photographs of the 500-element ultrasound array. **a**: Back of the array showing cabling. **b**: Front of the array. **c**: A block diagram of the experimental setup used for the sonications.

used to activate therapeutic agents (19) and occlude blood vessels (20).

In this study we utilized the information provided by prior studies and developed an MRI-compatible large focused ultrasound array system suitable for trans-skull sonications. The aim of this study was to test the array system for trans-skull thermal ablation of in vivo tissue using ex vivo human skulls and an animal model. This is an important extension of the prior work and is required before a clinical system is developed.

## MATERIALS AND METHODS

### Sonication System

A large hemispherical transducer array (Fig. 1a,b), similar in shape and size to that reported earlier (21), was constructed. Based on previously reported simulation studies (21), the array consisted of 500 equally sized elements. The array itself was custom-manufactured by Imasonics (Besancon, France) using 1–3 piezo-composite material. This material includes small piezo-ceramic pillars embedded in a polymer matrix (22). The piezoelectric material was covered with electrodes on both surfaces. The back electrode was divided into 500 equal area elements (element area  $2.8 \text{ cm}^2$ ). The piezo-composite material was then formed to a hemispherical shape (diameter 30 cm). The front electrode was connected to ground and the back electrodes to individual coaxial cables. The array was mounted in a fiberglass case and the front electrode was completely covered by an acoustic matching layer that also acted as an electrical insulator. Thus, all of the electrical connections were encased and waterproof. Copper was used in the cabling to avoid MRI artifacts. Each element had air backing. The array was operated at frequencies between 700 and 800 kHz. Array cabling, calibration, and testing were performed in-house using methods similar to those described earlier (21). A smaller nine-element array, with identical element size, shape, and material to the 500-element array, was used to estimate the conversion efficiency from RF to acoustic power using the radiation force method. This acoustic efficiency was determined to be  $\sim 60\%$ . The array was driven with a specifically developed 500-channel RF-amplifier system (InSightec, Haifa, Israel). The system allowed control of the phase and amplitude of

the driving RF-signal of each transducer element similar to systems reported earlier (23).

### Experiments

The experimental setup is shown in Fig. 1. The transducer was designed to be placed on its side so that its axis would be parallel to the magnet axis, thus allowing the head of a patient lying in an MRI scanner in a clinical treatment to be placed inside the hemispherical array. To simplify the experiments, the array was placed facing up and completely submerged in water in an acrylic tank. A formalin-fixed ex vivo human skull was mounted in a polycarbonate frame and attached to the array. The skull was filled with an ultrasound phantom material that simulates the acoustic properties of brain (24). In the middle of the brain phantom, a small space was hollowed out for the animal. To simulate the skin, the external surface of the skull was covered by a thin layer (2–3 mm) of the same phantom material. A thin plastic sheet over the phantom material protected it from the water and held it in place. Since the dominant factor influencing the beam propagation is the skull bone, the later experiments (two thighs and seven brains) were conducted without the skin phantom to simplify the setup. In the experiments where high-power sonications were tested, the brain phantom was replaced by degassed water to eliminate the potential for cavitation induced by gas trapped in the phantom material. This was found to be a problem in the initial high-power sonications.

The ultrasound wave front is distorted while it propagates through the skull bone. Two methods were used to determine the phasing scheme necessary to restore the focus within the skull. In the first method, a previously developed phase aberration correction algorithm which takes into account bone thickness, shape, and density (12) was used. Data for this phasing algorithm was obtained from a digitized 3D rendering of the skull with CT images (Siemens SOMATOM CT Scanner, FOV = 20 cm, slice thickness = 1 mm). The polycarbonate frame on which the skull was mounted had markers that were visible in the CT images. The frame was mounted to the transducer in a known location, so with these markers the CT and transducer coordinates were registered (12). The second

Table 1  
Sonication parameters for each location for the brains that were sonicated at high power levels

Rabbit #	Location	Acoustic power (W)	Duration (s)	Number of sonications
1	a	360	20	1
	b	1080	20	1
2	a	720	20	2
		1080	20	1
	b	1080	30	1
		720	20	2
3	a	1080	20	2
		600	20	1
	b	600	20	3
		720	20	1
4	a	720	30	1
		600	20	1
	b	720	20	1
		600	20	2
		600	30	2

The letters a, b, and c indicate different locations in the brain.

method to calculate the phase corrections used a needle hydrophone (Precision Acoustics, Dorchester, UK) placed in the geometric focus (inside the hollowed-out region in the phantom that filled the skull) (25). The elements were driven one at a time and the hydrophone signal was recorded by a computer and stored in a file for the sonications. Electric steering of the focus away from the initial focal point was tested using a previously described approach (25).

In most of the sonications the ultrasound focus was aimed at the geometric center of the phased array. After loading the phase corrections for each element, the sonications were started (20 or 30 sec, continuous wave). The amplitude of each array element was kept constant, so the power distribution was uniform on the transducer surface. The position of the focus was found by performing sub-threshold sonications and monitoring the temperature distributions with MRI at the depth determined in phantom sonications prior to the animal sonications. The hot spot was always visible in this image, and it was used to determine the location of the orthogonal image plane. Multiple high-power sonications were performed at each location (see Table 1). The beam was aimed at new locations by moving the animal. In one case the focus was electroni-

cally shifted around the geometric center of the phased array.

### Animal Preparation

The experiments were approved by our animal committee. New Zealand white rabbits (~4 kg, males) were anesthetized with a mix of 40 mg/kg ketamine (Aveco, Fort Dodge, IA), and 10 mg/kg of xylazine (Lloyd Laboratories, Shenandoah, IA). The hair on the skin over the target tissue was removed before the experiments and the animal was placed on a tray so that the target tissue was inside the skull at the focus. The animal body temperature was stabilized using a temperature-controlled vinyl pad through which warm water circulated. The rectal temperature was measured with a copper-constantan thermocouple. In the first test, the thigh muscle was sonicated (15 locations in three rabbits using two ex vivo human skulls). In the second set of experiments, the brain was sonicated. Just before the brain experiments, a craniotomy was performed to remove as much skull bone as possible. The skin was sutured back over the bone window and degassed saline was used under the skin to minimize the presence of gas. These experiments were performed in a total of 22 locations in 10 rabbits. In order to take into account the variation caused by variable skull thickness and density, three ex vivo human skulls were used in these experiments.

### MRI

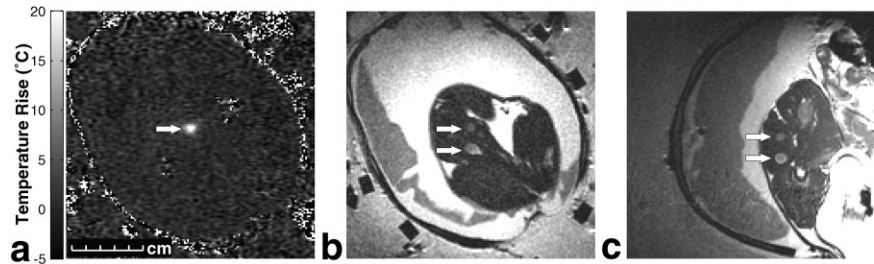
The whole setup was placed in a standard 1.5 T MRI scanner (Signa, General Electric Medical Systems, Milwaukee, WI). The temperature-dependent proton resonant frequency shift was measured by subtracting phase images obtained by a fast spoiled gradient echo sequence (FSPGR) (13) and using an experimentally measured temperature coefficient of 0.011 ppm/°C (26) (Table 2). The sonication began after the first (baseline) image was acquired. The absolute temperatures were calculated by adding the animal body temperature to the MRI-derived temperature elevation. The temperature values and images reported here were acquired immediately after the ultrasound was turned off. To evaluate the tissue damage after the sonications, a fast spin echo (FSE)  $T_2$ -weighted sequence was used in the muscle tissue. In the brain  $T_1$ -weighted images were obtained by using an FSE before and after an intravenous injection of a bolus of gadopentetate dimeglumine contrast agent (Magnevist, Berlex Laboratories, Wayne, NJ)

Table 2  
MRI parameters used in the study

Sequence	Purpose	Repetition time (ms)	Echo time (ms)	Matrix	Flip angle (Deg)	Bandwidth (kHz)	Number of echoes	Number of acquisitions
FSPGR	Temperature measurement	39.9	19.7	256 × 128	30	3.57	1	1
FSE $T_1$ -W	Tissue damage in brain	500	15	256 × 256	90	16	4	2
FSE $T_2$ -W	Tissue damage in muscle, brain	2000	75	256 × 256	90	16	8	2

FSPGR = Fast spoiled gradient echo sequence; FSE  $T_1$ -W = Fast spin echo  $T_1$ -weighted sequence; FSE  $T_2$ -W = Fast spin echo  $T_2$ -weighted sequence.

FIG. 2. **a:** MRI-derived temperature map (across the focal plane) acquired at the end of a 20-sec sonication in the rabbit thigh showing the focal heating (arrow). **b,c:**  $T_2$ -weighted FSE images (TR/TE = 2000/70 ms) of two thermal lesions (arrows). **a,b:** Image across the focal plane. **c:** Perpendicular orientation.



(dose 0.2 mmol/kg). All of the imaging parameters are reported in Table 2. Because of the high contrast between normal tissue and tissue treated with focused ultrasound, no grading scheme was used to determine whether the tissue was damaged. All MRI-related analyses were performed by one author using software written in-house.

In order to improve the signal-to-noise ratio, a surface coil with a diameter of 18 cm was placed on top of the animal during the sonications. After the brain sonications, additional imaging was performed with a 7.5 cm coil under the head to create a more detailed image of the brain and the ultrasound-induced damage. This coil provided us good lesion detection in the small rabbit brain and thus assured that there was no unexpected tissue damage outside the focus. For the phantom experiments in the clinical orientation (described below), only the body coil was used to simulate the clinical treatments.

#### Histology Preparation

The animals were euthanized immediately after the experiments with an i.v. injection of sodium pentobarbital. The brains were removed and fixed in 10% buffered formalin, then embedded in paraffin and sectioned serially at 6  $\mu\text{m}$ . Hematoxylin and eosin (H&E) was used to stain the sections before evaluation under a light microscope. The area of the resulting lesions in the stained sections was estimated by measuring the width of the lesions in two perpendicular directions. In the thigh experiments, the damage to muscle was detected only by using  $T_2$ -weighted imaging, as it has been shown to correlate well with the histology-detected tissue coagulation (27). All histology-related analysis was performed by one author (NV).

#### Phantom Tests in a Clinical Orientation

After the animal tests the system was modified so that it could operate in the orientation that will be used clinically. The array was mounted on its side and the opening was covered by a latex membrane with a hole cut in the middle. The hole was large enough to be stretched around a human head and attached with adhesive tape to provide a water-tight seal. The functionality of this membrane was verified in tests with a volunteer. The system was designed so that the top part of the head will be in the opening of the array with the target location in the geometric focus of the hemisphere. The space between the skin and the array is then filled with degassed temperature-controlled water. To test this approach, a human skull sample was filled with ultrasound phantom material (as described above) and mounted to a cylindrical plastic holder. The holder was

fixed in place by mounting it to a base that was fixed to the MRI table. The latex membrane was fixed to the edge of the array and the hole in the membrane was sealed around the plastic holder. The array was then filled with water and sonications through the skull were performed into the phantom while acquiring MRI temperature elevation maps. The water circulation system provided degassed, temperature-controlled water circulation and was interrupted during the sonications. The array was aimed based on FSE images showing the geometry of the array along the coronal and sagittal planes. The accuracy of the targeting was determined by measuring the distance of the hot spot as measured from the MR thermometry images from the intended location. A total of 82 sonications were performed at 17 different locations inside the skull. The body coil was used for MRI during these experiments.

## RESULTS

### Muscle Sonications

Sharply focused heating was induced in the rabbit thigh through the human skull (Fig. 2a). There was a clear difference in the MRI-measured heating between the uncorrected and phase-corrected sonications (Fig. 3a–c). In one thigh, for example, the average temperature elevation/applied acoustic power of two 20-sec sonications was  $0.092^\circ\text{C/W}$  and  $0.077^\circ\text{C/W}$  for the hydrophone and the model-based sonications, respectively. A sonication without correction yielded  $0.053^\circ\text{C/W}$  in the same thigh. The average temperature elevation for 12 hydrophone-corrected sonications in three rabbits (two skulls) was  $0.04 \pm 0.03^\circ\text{C/W}$ , demonstrating the variability of the temperature elevation and the need for online temperature measurement. Figure 3d–f demonstrates the ability of electronically shifting the focus. The focus could be electronically steered by  $\sim 5$  mm, but the magnitude of the temperature elevation was reduced. This reduction was expected based on the ultrasound field-predicted behavior implied by the size of the transducer elements and was confirmed by measurements with this device (12).

At the higher power levels (applied acoustic power 600–1080 W), the sonications caused thermal lesions which were detected in  $T_2$ -weighted images (Fig. 4a,b). A total of 15 locations were sonicated in three animals. Tissue damage at the focal locations was observed in all but two cases. In one case the  $T_2$ -weighted imaging performed immediately after the sonication did not detect a lesion. In the other, it was found that the hair over that location was not completely removed, inducing skin heating. Skin heating was also seen in one low-power sonication (excluded from

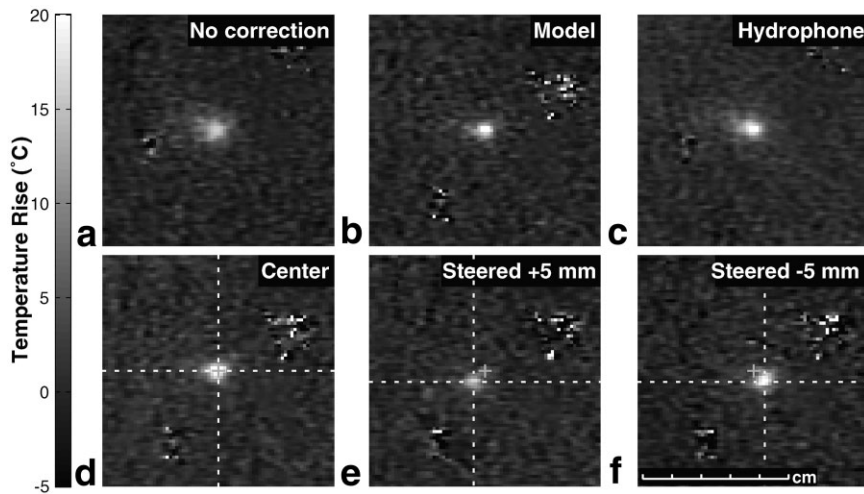


FIG. 3. MRI-derived temperature maps acquired at the end of six 20-sec sonications in rabbit thigh muscle. **a–c**: Examples of heating with and without phase correction. **a**: No phase correction. **b**: Correction determined with ultrasound propagation model that used bone properties derived from CT scans. **c**: Correction determined by placing a hydrophone at the focus before the animal experiments. **d–f**: Electronic beam steering. **d**: Focus at the geometric center of the array. **e,f**: Focus electronically shifted  $\pm 5$  mm away from the location in **d**. The target locations were selected to be in directions that are at a  $90^\circ$  angle to each other to show this ability in the two axial directions. Dotted lines: targeted locations. Cross: geometric center of the array.

temperature analysis) that had the center of the focal region only 5 mm from the skin.

#### Brain Sonications

The brain sonications also resulted in sharp temperature elevations (Fig. 4a,b). All of the sonications produced an average temperature rise of  $0.022 \pm 0.010^\circ \text{C/W}$ . A series of sonications at different power levels without the phantom material were performed in nine locations in four rabbits. First the low-power sonications were used to establish the location of the focus and then a series of higher-power sonications were delivered with increasing power, as shown in Table 1. All of these sonications produced sharp focal temperature elevations. MRI (Fig. 4c–e) and histology (Fig. 6) examination of the brains revealed lesions at the focal locations except in the location of the lowest-power level (360 W). For all of the sonications the histologically measured lesion area correlated with the

achieved peak temperature, but not with the applied acoustic power (Fig. 5). The tissue damage appeared either as areas of coagulation necrosis induced by threshold-level heating or as areas of high-temperature coagulation necrosis. Figure 6 shows an example of the microscopic appearance of a lesion.

#### Phantom Experiments in a Clinical Orientation

The phantom experiments showed clearly that the array can operate in the position that will be used clinically. Figure 7a shows an image of the phantom, skull, and array, demonstrating that any MR image distortion caused by the device is minimal and that it is possible to image the whole human head while in the array. The experiments also showed that the method resulted in good acoustic coupling, since water filled the entire path of the ultrasound beam from the array surface to the skull (Fig. 7a). The focal spot was clearly visible in the MR thermometry

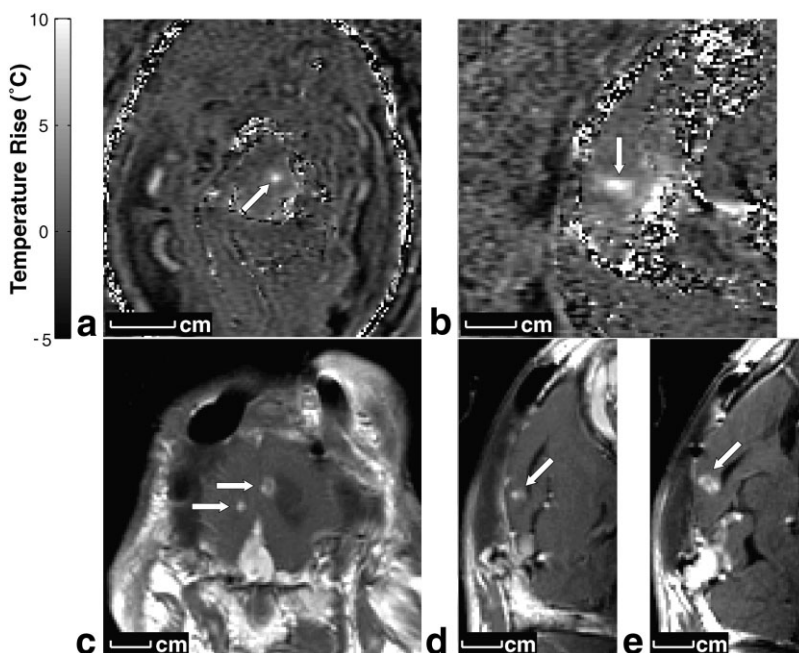


FIG. 4. **a,b**: MRI-derived temperature images acquired at the end of 20-sec sonications in the rabbit brain. **c–e**: Contrast-enhanced  $T_1$ -weighted images (500/15) of two thermal lesions in a rabbit brain. The images in **a** and **c** were acquired across the beam at the focal plane; **b,d,e** were acquired in the perpendicular orientation (along the axis of the array). **c–e** were acquired using a 7.5 cm diameter surface coil after moving the animal from the sonication system.

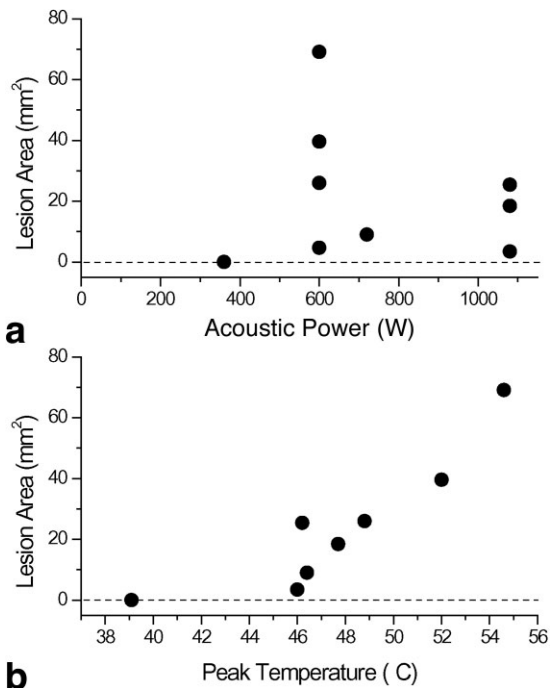


FIG. 5. The brain lesion area measured from the histology slides as a function of the highest applied acoustic power (a) and highest induced temperature (b). One location was not plotted in the temperature graph due to motion during the sonication.

images during the sonications (Fig. 7b–e). The standard deviation of the noise was  $\pm 2.1^{\circ}\text{C}$  during these sonications and  $\pm 1.3^{\circ}\text{C}$  when the sound was off. The average error in targeting was  $3.2 \pm 1.5$  mm (mean  $\pm$  SD).

## DISCUSSION

These results extend those of previous simulation studies (28) and those that performed ultrasound field measurements in a water tank with ex vivo samples (12) in dem-

onstrating that sharp pressure field focusing can be accomplished through the human skull using phased arrays. In this study, a significant step towards clinical feasibility was taken by developing an MRI-compatible phased array system and demonstrating sharp temperature elevations and focal tissue coagulation in in vivo perfused tissues through human skulls. The measured temperature elevations were highly localized, and the induced tissue damage showed a sharp boundary between the lesions and undamaged tissue similar to what has been observed after sonications performed through a bone window (15,26). The lesions found after the sonications are consistent histologically with the tissue damage observed in previous MRI-guided focused ultrasound studies (16,29). No damage that is usually associated with cavitation events (29), such as hemorrhage and mechanical damage to the blood vessels, was found. Overall, the finding of these experiments continue to support the hypothesis that completely noninvasive MRI-guided thermal coagulation of brain is possible using large ultrasound phased arrays.

In these experiments the applied acoustic power did not correlate well with the lesion size. This result is expected, since the attenuation and reflection in the skull is strongly location-dependent and results in substantial variation to the focal pressure amplitude (12). However, the peak temperature elevation did correlate well with the induced lesion size. The actual temperature threshold appeared slightly lower than what is expected based on earlier work (30,31), and was most likely due to the fact that the peak temperatures were measured after the sound was turned off and that the measurements were averaged over the 3-mm thick imaging slice thickness, which may have reduced the measured peak temperature. Nevertheless, these results agree with earlier studies (30) in that the power alone is not a good predictor for the resulting tissue coagulation, and that online temperature monitoring can be used as a guide to assure that adequate temperatures have been achieved.

FIG. 6. Photomicrographs of two H&E-stained sections of lesions in the rabbit brain produced during sonications through a human skull sample. a–c: Small lesion near the thermal threshold for tissue damage appears as a light stained area (arrows) under low-power magnification a. b: Details of the central area reveal nuclear condensation in the central area (b) and vacuolation at the margin (c). d–f: Two high-temperature thermal lesions in the cortex. e: Lamination of the lesion region. f: High-temperature coagulation of the neuropil in the solid central core.

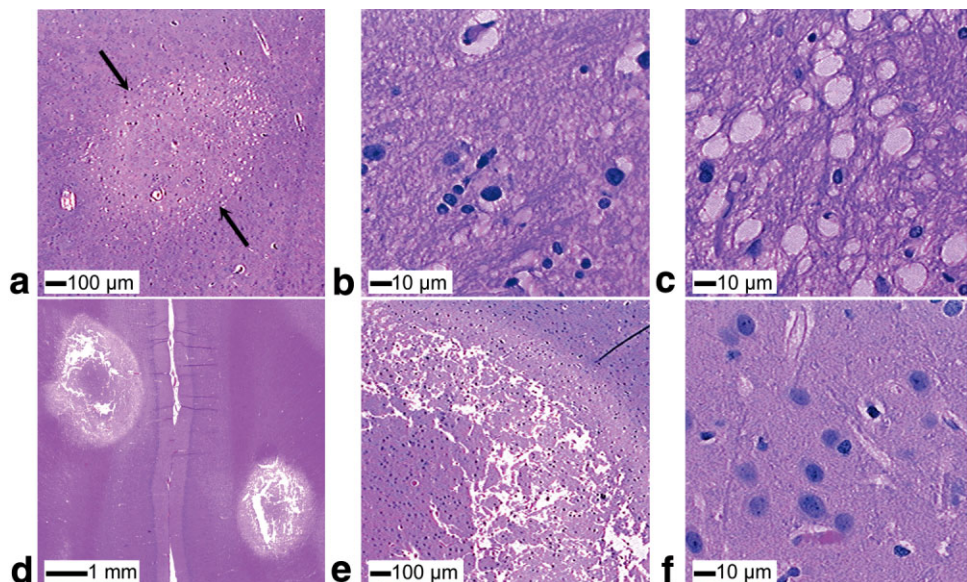
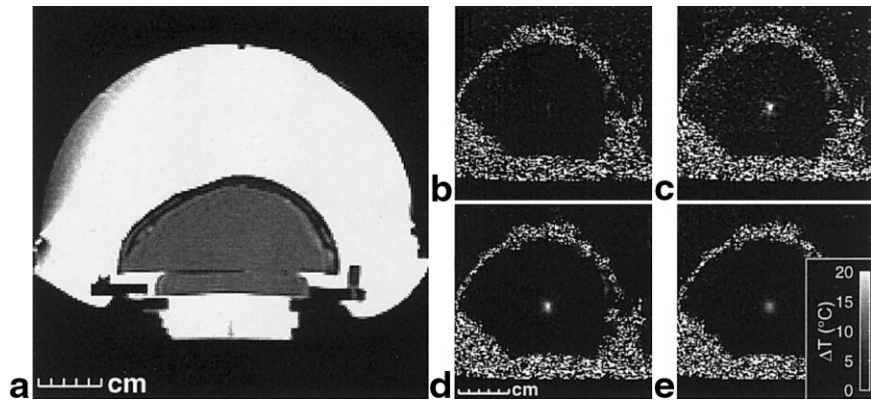


FIG. 7. Operation of the focused ultrasound system in a clinical orientation. The transducer was mounted on its side and a water seal was produced by a flexible membrane. **a**:  $T_2$ -weighted image showing the phantom-filled skull mounted inside the array filled with water. **b–e**: Temperature images acquired during one 20-sec sonication (acoustic power: 500 W). The images in **b,c** were acquired during the sonication (2.7 sec and 18.8 sec into the sonication, respectively), and the images in **d,e** were acquired 9.2 sec and 19.8 sec after the power was turned off.



In these experiments, only the phase of the ultrasound wave was corrected for the bone-induced distortions; amplitude variations were not considered. By considering the actual ultrasound-induced attenuation and the pressure at the focus, a better correlation between the applied power and the lesion sizes may have been achieved. However, the temperature elevation was smaller in the brain than in the muscle in the same experimental conditions and through the same skulls. This difference is expected, since the ultrasound absorption coefficient in brain is lower and the blood perfusion rate higher than in muscle, both factors that decrease the temperature elevation. The findings here, along with previous work (3), continues to clearly demonstrate that the uncertainty in ultrasound attenuation and blood perfusion rate (which will vary especially in a tumor) will influence the achieved temperature rise. The findings thus demonstrate the need for online temperature monitoring during clinical ultrasound brain surgery.

Two methods were tested to correct the distortions induced by the skull on the ultrasound field. The hydrophone method (25) produced higher temperatures than the model-based correction. However, the downside of this method is that it would require the invasive introduction of a hydrophone in a clinical treatment. The least invasive way to do this would be to use intravascular catheters, as proposed earlier (25). The completely noninvasive model-based method also resulted in good focusing. The difference between the two methods is consistent with what was found before in a study where the acoustic field was mapped in water (32). There are more complex models under development that take into account the 3D structure of the bone (33) and should provide better model-based focusing. In addition, the use of a nonlinear relationship between the ultrasound speed and the bone density may improve the results (33). However, the model-based focusing could not be better than that achieved by the hydrophone-based focusing and will thus require more acoustic power. In the case of the methods used in this study, the difference was  $\sim 30\%$ .

The two cases where skin burns were produced when sonicating muscle require further explanation. In the first, the ultrasound beam was focused close to the skin. Since the ultrasound amplitude attenuation coefficient is much higher in the skin (14–66 Np/m at 1 MHz) than muscle (4–15 Np/m at 1 MHz) (34) and the incident angles were high for most of the beam when the focus was shallow,

these burns are not surprising. In the other case, some hair was left on the skin, resulting in high attenuation. In both cases the skin was located inside the human skull sample and very close to the focal spot. Therefore, these results do not indicate that similar skin burns would be induced in patient treatments where the focus would be located several centimeters away from the skin.

Our phantom experiments showed that the ultrasound beam can be coupled to a patient's head in an orientation that will allow clinical treatments. In addition, they showed that the array is not distorting the MR image to a degree that would prevent the whole brain imaging. The sonication accuracy that was achieved by imaging the array and using the image to register the array coordinates was on the order of the imaging slice thickness and small enough to allow the focus to be safely placed within a tumor with a diameter of 10 mm or more. The first sonication will be performed at low power to aim the beam and then adjustments can be made so that precise focal spot tissue coagulation can be achieved. The noise associated with the MRI thermal images that was present in the animal sonications was reduced by filtering, so that thermometry could be performed during the sonications. Temperature elevations 5–7°C were clearly visible during these sonications. These exposures are low enough not to induce any tissue damage (15) and can thus be used to target the sonications. Based on these results, this hemispherical ultrasound phased array system may be useful for noninvasive brain tumor coagulation. However, before clinical trials are performed, the whole system needs to be tested with a large animal model such as monkeys that would allow close to human size testing of the whole procedure.

## REFERENCES

1. Foster RS, Bihrlé R, Sanghvi NT, Fry FJ, Donohue JP. High-intensity focused ultrasound in the treatment of prostatic disease. *Eur Urol* 1993;23:29–33.
2. Chapelon JY, Ribault M, Vernier F, Souchon R, Gelet A. Treatment of localised prostate cancer with transrectal high intensity focused ultrasound. *Eur J Ultrasound* 1999;9:31–38.
3. Hynynen K, Pomeroy O, Smith DN, Huber PE, McDannold NJ, Kettenbach J, Baum J, Singer S, Jolesz FA. MR imaging-guided focused ultrasound surgery of fibroadenomas in the breast: a feasibility study. *Radiology* 2001;219:176–185.
4. Lynn JG, Putnam TJ. Histology of cerebral lesions produced by focused ultrasound. *Am J Pathol* 1944;20:637–652.
5. Fry WJ, Barnard JW, Fry FJ, Krumins RF, Brennan JF. Ultrasonic lesions in the mammalian central nervous system. *Science* 1955;122:517–518.

6. Lele PP. A simple method for production of trackless focal lesions with focused ultrasound: physical factors. *J Physiol* 1962;160:494–512.
7. Heimburger RF. Ultrasound augmentation of central nervous system tumor therapy. *Indiana Med* 1985;78:469–476.
8. Daum DR, Hynynen K. A 256 element ultrasonic phased array system for treatment of large volumes of deep seated tissue. *IEEE Trans Ultrason Ferroelect Freq Contr* 1999;46:1254–1268.
9. Daum D, Buchanan MT, Fjield T, Hynynen K. Design and evaluation of a feedback based phased array system for ultrasound surgery. *IEEE Trans Ultrason Ferroelect Freq Contr* 1998;45:431–438.
10. Hynynen K, Jolesz FA. Demonstration of potential noninvasive ultrasound brain therapy through intact skull. *Ultrasound Med Biol* 1998;24:275–283.
11. Thomas J-L, Fink MA. Ultrasonic beam focusing through tissue inhomogeneities with a time reversal mirror: application to transskull therapy. *IEEE Trans Ultrason Ferroelect Freq Contr* 1996;43:1122–1129.
12. Clement GT, Hynynen K. A non-invasive method for focusing ultrasound through the human skull. *Phys Med Biol* 2002;47:1219–1236.
13. Ishihara Y, Calderon A, Watanabe H, Okamoto K, Suzuki Y, Kuroda K. A precise and fast temperature mapping using water proton chemical shift. *Magn Reson Med* 1995;34:814–823.
14. Salomir R, Vimeux FC, De Zwart JA, Grenier N, Moonen CW. Hyperthermia by MR-guided focused ultrasound: accurate temperature control based on fast MRI and a physical model of local energy deposition and heat conduction. *Magn Reson Med* 2000;43:342–347.
15. Hynynen K, Vykhodtseva NI, Chung A, Sorrentino V, Colucci V, Jolesz FA. Thermal effects of focused ultrasound on the brain: determination with MR Imaging. *Radiology* 1997;204:247–253.
16. Chen L, Bouley D, Yuh E, D'Arceuil H, Butts K. Study of focused ultrasound tissue damage using MRI and histology. *J Magn Reson Imag* 1999;10:146–153.
17. Hynynen K, McDannold N, Vykhodtseva N, Jolesz FA. Noninvasive MR imaging-guided focal opening of the blood-brain barrier in rabbits. *Radiology* 2001;220:640–646.
18. Siegel RJ, Cumberland DC, Myler RK, DonMichael TA. Percutaneous ultrasonic angioplasty: initial clinical experience. *Lancet* 1989;2:772–774.
19. Umemura S-I, Kawabata K-I, Sasaki K. In vitro and in vivo enhancement of sonodynamically active cavitation by second-harmonic superimposition. *J Acoust Soc Am* 1997;101:569–577.
20. Delon-Martin C, Vogt C, Chigner E, Guers C, Chapelon JY, Cathignol D. Venous thrombosis generation by means of high-intensity focused ultrasound. *Ultrasound Med Biol* 1995;21:113–119.
21. Clement GT, Sun J, Giesecke T, Hynynen K. A hemisphere array for non-invasive ultrasound brain therapy and surgery. *Phys Med Biol* 2000;45:3707–3719.
22. Chapelon JY, Cathignol D, Cain C, Ebbini E, Kluiwstra JU, Sapozhnikov OA, Fleury G, Berriet R, Chupin L, Guey JL. New piezoelectric transducers for therapeutic ultrasound. *Ultrasound Med Biol* 2000;26:153–159.
23. Daum DR, Buchanan MT, Fjield T, Hynynen K. Design and evaluation of a feedback based phased array system for ultrasound surgery. *IEEE Trans Ultrason Ferroelect Freq Contr* 1998;45:431–438.
24. D'Souza WD, Madsen EL, Unal O, Vigen KK, Frank GR, Thomadsen BR. Tissue mimicking materials for a multi-imaging modality prostate phantom. *Med Phys* 2001;28:688–700.
25. Clement GT, Hynynen K. Micro-receiver guided transcranial beam steering. *IEEE Trans Ultrason Ferroelect Freq Control* 2002;49:447–453.
26. Vykhodtseva N, Sorrentino V, Jolesz FA, Bronson RT, Hynynen K. MRI detection of the thermal effects of focused ultrasound on the brain. *Ultrasound Med Biol* 2000;26:871–880.
27. Hynynen K, Darkazanli A, Unger E, Schenck JF. MRI-guided noninvasive ultrasound surgery. *Med Phys* 1993;20:107–115.
28. Sun J, Hynynen K. The potential of transskull ultrasound therapy and surgery using the maximum available skull surface area. *J Acoust Soc Am* 1998;104:2519–2527.
29. Vykhodtseva NI, Hynynen K, Damianou C. Histologic effects of high intensity pulsed ultrasound exposure with subharmonic emission in rabbit brain in vivo. *Ultrasound Med Biol* 1995;21:969–979.
30. McDannold NJ, King RL, Jolesz FA, Hynynen KH. Usefulness of MR imaging-derived thermometry and dosimetry in determining the threshold for tissue damage induced by thermal surgery in rabbits. *Radiology* 2000;216:517–523.
31. Vykhodtseva N, Sorrentino V, Jolesz FA, Bronson RT, Hynynen K. MRI detection of the thermal effects of focused ultrasound on the brain. *Ultrasound Med Biol* 2000;26:871–880.
32. Clement GT, Hynynen K. Correlation of ultrasound phase with physical skull properties. *Ultrasound Med Biol* 2002;28:617–624.
33. Connor CW, Clement GT, Hynynen K. A unified model for the speed of sound in cranial bone based on genetic algorithm optimization. *Phys Med Biol* 2002;47:3925–3944.
34. Goss SA, Johnson RL, Dunn F. Comprehensive compilation of empirical ultrasonic properties of mammalian tissues. *J Acoust Soc Am* 1978;64:423–457.